Available online www.jsaer.com

***Journal of Scientific and Engineering Research*, 2019, 6(11):258-266**

Research Article

ISSN: 2394-2630
CODEN(USA): JSERBR

Investigation of the tectonic structure of Saros Gulf with the help of geophysical data

A. Muhittin ALBORA

İstanbul University-Cerrahpaşa, Engineering Faculty, Geophysical Department, 34850, Avcılar, İstanbul, Turkey
Email: muhittin@istanbul.edu.tr

Abstract In this study, Steerable Fılters with current applications in electronic engineering are used to determine discontinuity limits in geophysics. Steerable Fılters are band-pass filters in a certain direction. The edges in different directions in an image are obtained by separating the image into the orientation subbands after passing through the basic filters with different directions. In this study, Steerable Fılters were applied to gravity anomaly map obtained in Saros Gulf and the results were compared with shallow and deep seismic sections obtained in Saros Gulf. Later, the connection between benthic formations and fault lines was made. Finally, the relationship between the fault lines with seismic activity of the region was investigated.

Keywords tectonic structure, geophysical data

Introduction

Research and identification of active faults is very important in terms of geology. There are several ways to detect faults. Geological methods, remote sensing methods, geophysical methods, etc. like. The identification of most active faults is very weak geologically, structurally or tectonically since there are no signs on the surface. Remote sensing methods can be effective in identifying and identifying active faults. Geophysical methods can provide effective methods for defining a large number of technical faults in land or marine environments and forming their geometries. Even the presence of faults under the surface or covered by current sedimentary structures is not a problem for geophysical methods. As an example of geophysical methods, both current and out of date faults can be determined by using seismic methods using sound wave conduction properties. The gravity method, which is applied by using mass density differences on the lateral surfaces of the fault after slip or slip, is very important for the determination of fault zones. It first finds local masses with greater or lower density than the surrounding units. It can be quite difficult to identify a unique source for an observed anomaly. The anomaly maps generated from the gravity data contain a number of features superimposed on each other. İnterpretation of such data aims to obtain useful information from the data. The identification and sketching of continuities in geosciences provides potential field geophysicists with important information to interpret gravity data. One of many techniques is Steerable Fılters with band-pass filter properties in specific directions, used in image processing such as bounding, image compression and enhancement, and texture analysis. The edges oriented in different directions can be obtained by separating the Steerable subbands obtained by applying the basic filters in different directions. Saros graben was selected as the study area. The high area created by the right lateral strike slip fault and reverse slip Anafartalar Fault, which developed as a positive flower structure during the late Upper Miocene-Early Pliocene form the southern margin of the Saros Graben, hinders the connection of the Dardanelles Strait [1]. Saros Bay is located in the NW Turkey. To the south is the Gelibolu Peninsula and to the north is Thrace. When the tectonic and geological features are considered, it combines the

North Aegean pit of the Ganosdağ basin, which is composed of active faults, and the continuation of the North Aegean pit. The Saros basin, which is approximately 60 km long and has seismic activity, extends in the SW-NE direction between Sporadhes basin in the North Aegean Trench and the Marmara Sea basin. It has a tectonic conformity with the right lateral pulsed seismically active transform fault North Anatolian Fault (NAF) [2]. It shows that the NAF is divided into several fault branches defining a tectonic region associated with high seismicity, passing through and south of the Sea of Marmara and progressing westward towards the north of the Aegean Sea. The NAF is located to the south of the Marmara Sea, the Gulf of Saros and the North Aegean Pit. Stress and depression areas in the region are formed by lateral strike-slip faults with vertical components [2]. In this study, Steerable Fılters are used to solve some problems in geophysical engineering. Using this method, it is aimed to locate buried faults from Bouguer anomaly map. Gravity anomaly map obtained by MTA of Saros Gulf region was studied as field study. In many image processing applications, such as edge detection, image compression and enhancement, and texture analysis, Steerable Fılters are basically band-pass filters in a certain direction. The edges with different orientations in an image can be obtained by passing the image through basic filters with different orientations and dividing the image into orientation subbands. In this, regard [3-7]. Many researchers have worked.

Methods

In many image processing applications such as edge detection, image compression and enhancement, and texture analysis, Steerable Fılters are basically band-pass filters in a certain direction. The edges with different orientations in an image can be obtained by passing the image through basic filters with different orientations and dividing the image into the orientation subbands. Figure-1 shows the guided filter block diagram that performs this process.

Here, $h^{\theta_1}(x,y)$, $h^{\theta_2}(x,y)\ldots,h^{\theta_M}(x,y)$ $h(x,y)'\ \theta_i$, $0\le i\le M$, values are the impulse responses of the filters corresponding to their returned state. The input image is separated into subband M using these filters so that the edges in the orientation corresponding to the orientation of the filters are determined.

If the expression of a $h(x,y)$ function at a random rotation value can be written in the form of a linear combination of the expressions at constant rotation values, this function is called a guided function. The mathematical expression of such a function is given in the following equation.

$$h^{\theta_a}(x,y)=\sum_{i=1}^{M}k_i(\theta_a)h^{\theta_i}(x,y) \tag{1}$$

$h^{\theta_a}(x,y)$, $h(x,y)'\ \theta_a$ corresponds to the returned state. $k_i(\theta_a)$, $0\le i\le M$, controlling the filter for the interpolated function.

$$e^{jl\theta_a}=\sum_{i=1}^{M}e^{jl\theta_i}k_i(\theta_a),\qquad 0\le l\le N, \tag{2}$$

condition, the routing functions can be switched to the Fourier Series as follows.

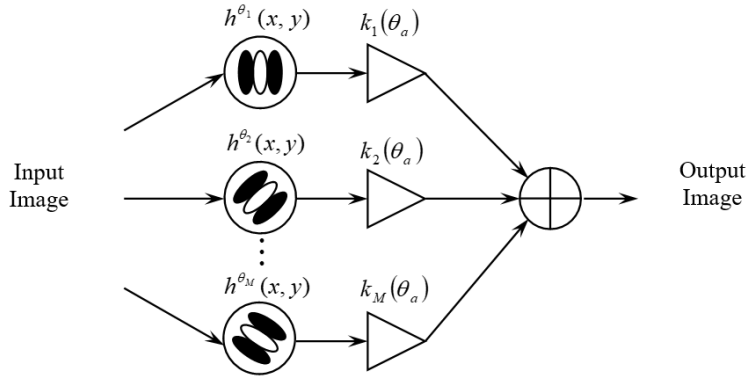

Figure 1: Block diagram of steerable filter [6]

$$h(r,\theta) = \sum_{n=-N}^{N} a_n(r) e^{jn\theta_a} \quad (3)$$

Here, $r = \sqrt{x^2 + y^2}$ and $\theta = \arg(x, y)$' and $x = r\cos\theta$, $y = r\sin\theta$ can be written as.

After determining the basic functions and interpolation functions, $h(x, y)$, corresponding to the rotated state of $h^{\theta_a}(x, y)$' θ_a, can be found using [Correlation-1]. Thus, the determination of the edges in the θ_a orientation in an image is achieved by passing this image through the $h^{\theta_i}(x, y)$ filters.

The energy in the θ_a direction can be calculated using the band-pass filters directed to the θ_a angle, using the conjugate of four. This is called directed energy. In order to calculate the directed energy function, $h^{\theta_a}(x, y)$ has to have the basic functions that make up the quadratic conjugate (these functions are Hilbert transformations of each other) [3]. The directed energy is calculated by the following expression using quadratic paired filters.

$$E^{\theta_a} = \left[f(x, y) * h^{\theta_a}(x, y)\right]^2 + \left[f(x, y) * g^{\theta_a}(x, y)\right]^2 \quad (4)$$

In this equation, "*" indicates the convolution process. $f(x, y)$ is the Hilbert transformation of the input image and $g^{\theta_a}(x, y)$ $h^{\theta_a}(x, y)$. The equation given by correlation-4 is opened to Fourier series as follows.

$$E^{\theta_a} = C_1 + C_2\cos(2\theta_a) + C_3\sin(2\theta_a) + \ldots \quad (5)$$

If the local dominant orientation θ_d resistance and S resistance are written using the low frequency terms in (Correlation-5),

$$\theta_d = \frac{1}{2}\tan^{-1}\left(\frac{C_3}{C_2}\right), \quad S = \sqrt{C_2^2 + C_3^2} \quad (6)$$

equation is obtained. The orientation map of an image can be created by calculating θ_d and S for each pixel in the image.

After creating the angle and the corresponding energy weight coefficient maps showing the orientation of each pixel of an image, the sum of the energies corresponding to each angle value from these two maps forms the angle-energy histogram of that image [6-7].

Tectonic and geological structure of the region

The NAF entered the Sea of Marmara with great earthquakes and changed the geography and tectonic structure of the region. After this mobilization, both large and small faults were formed both on land and in the sea. Many scientists have argued that the waters of the Mediterranean Sea entered the Gulf of Saros and formed the Sea of Marmara, which was previously a lake. For this reason, many authors treat and examine the Aegean Sea as part of the Mediterranean Sea. However, the geological and tectonic structure of the Aegean Sea is quite different and complex than the rest of the Mediterranean Sea. The Gulf of Saros is one of the deepest parts of the Aegean Sea and is dominated by block-shaped faulting. During the Late Upper Miocene-Early Pliocene period, the right-sided lateral strike slip fault and reverse slip Anafartalar Fault, which form the southern edge of the Saros Graben, developed as a positive flower structure prevented the previous connection around Saros Bay [1]. The connection of these elevations has prevented the connection in the region that corresponds to the Dardanelles [1]. They suggested that the fault bounding the northern side of the Saros Gulf constitutes the right lateral strike-slip northern branch of the North Anatolian Fault during the young Middle Miocene-Late Miocene period [1]. There are five main structural elements in the Gulf of Saros and its vicinity from northwest to southeast: Hisarlidağ Rise, Enez Graben, Semadirek Rise, Saros Graben and Gallipoli Block. The development of the stress and depression areas in this region is caused by lateral strike-slip faults with vertical components. Looking at the geology and tectonics of the Saros Gulf, it is seen that the Ganos Mountain Basin, which is composed of active faults, connects the North Aegean Pit to the Marmara Sea (Figure 2). The Saros Basin extends in the SW-

NE direction between the Marmara Sea Basin and the Sporafdhes Basin in the Northern Aegean Trench. The basin also forms a tectonic association with a seismic activity of 1500 km in length with a right lateral strike-slip transform fault (NAF) [8]. The NAF is divided into several fault branches defining a tectonic region associated with high seismicity as it travels westward towards the north of the Aegean Sea, passing through and south of the Sea of Marmara [9-11]. The development of the stress and depression areas in this region is caused by lateral strike-slip faults with vertical components. He states that the faults bordering Saros Graben include lateral movements along with vertical movements [12]. These characteristics are also seen in the gravity anomaly maps of this region [13-14].

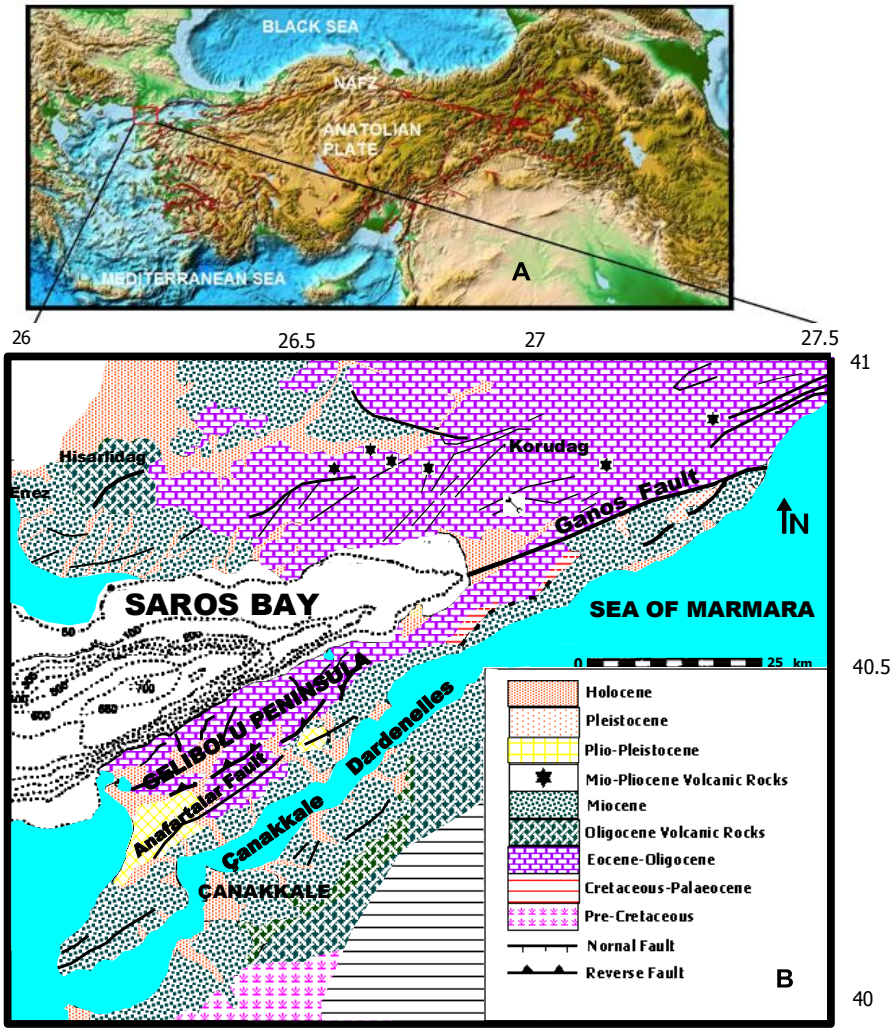

Figure 2: Working area A) Turkey map B) Saros region's geology and bathymetry map (modified from [15])

Seismicity

When the bathymetry of the Gulf is examined, it is observed that the secondary canyons in the canyon are cut at the sea floor and shifted to the right side (Figure 3). İt supports the right lateral movement of the faults by fault solutions belonging to the earthquakes in Saros Bay. Mw = 6.7 magnitude earthquake solution [16] occurred in the Gulf in 1975 and fault solutions of the largest earthquake in 2003 (Mw = 5.7) [17] show the strike-slip result (Figure 3). These earthquakes also support the approach that the Ganos Fault is the main fracture causing an earthquake in the Gulf of Saros and has a right lateral strike slip fault character. When the thickness of the young sediment packets in the internal depression is examined, it is observed that only the top sediment pack thickness increases and there is no change in thickness (Figure 3) [18].

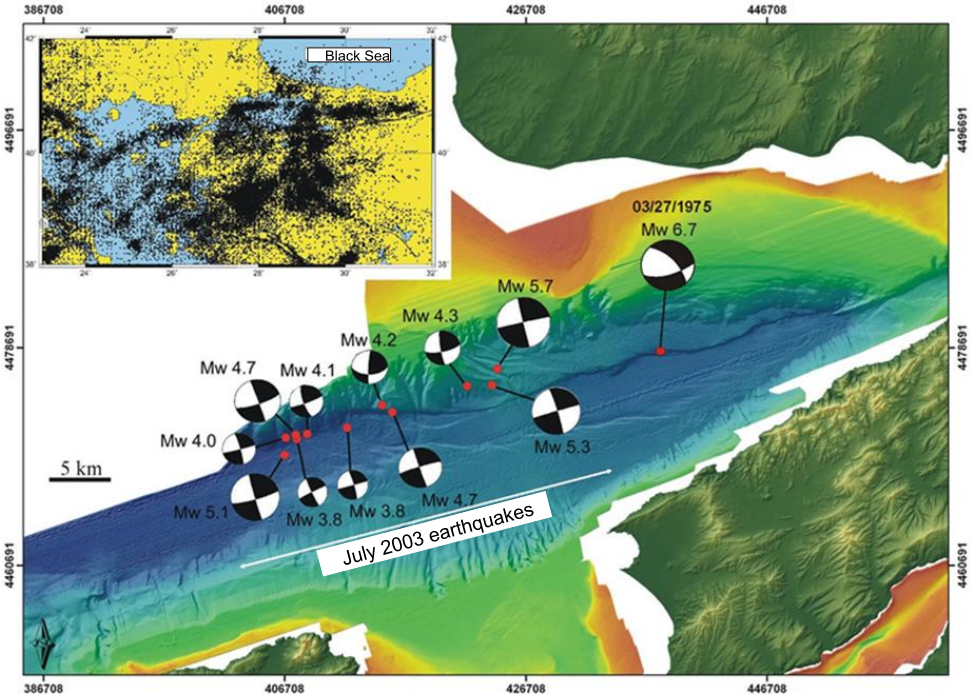

Figure 3: The relationship between Ganos fault and the location of the earthquake occurring in March 1975 and July 2003 in the Gulf of Saros [16-18]

Application of Method to Area Data

The General Directorate of Mineral Research and Exploration (M.T.A.) prepared the gravity anomaly maps used in the study in 1989. Turkey's Bouguer gravity anomaly map values decrease from west to east. The zero contour of Bouguer gravity anomaly follows the extension of the NAF to the east of the Sea of Marmara. reaches the depth of the steep morphological pits and pits filled with sedimentary cover caused by low gravity values showing the North Aegean pit continues [19-20]. Figure 3 shows the location of Saros Bay and seismic activity in the region [21]. When the Bouguer Gravity anomaly map is examined (Figure 4), an anomaly value of approximately 70 mgal was observed on the Saros Graben. The gravity anomaly map output of the gravity anomaly map given in Figure 4 is obtained by applying the Steerable Filter method and is shown in Figure 5. This value also shows the maximum gravity value in the region. Gravity values gradually decrease in northwest-southeast directions. İn this study, the borders and geometries of geological structures causing these anomalies were investigated by using 0 °, 45 ° and 135 ° filters (Figure 5).

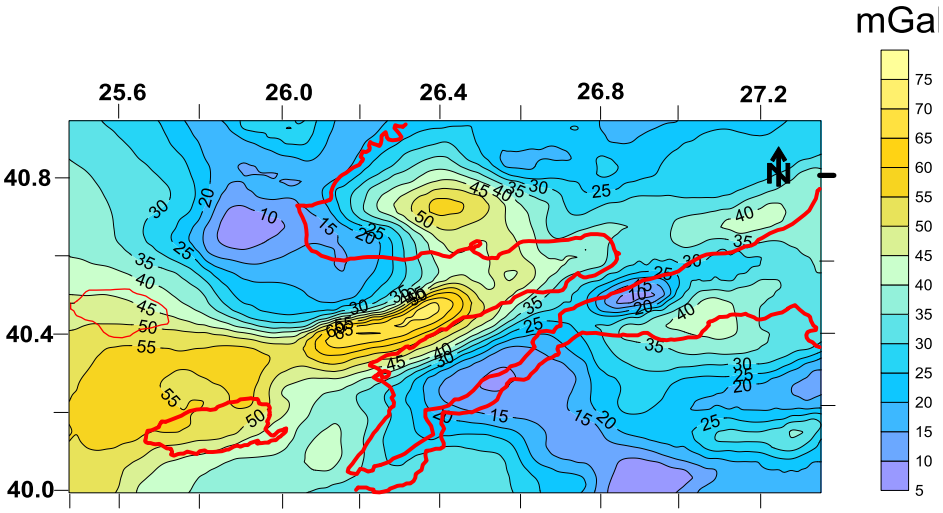

Figure 4: Bouguer anomaly map of Saros Gulf (taken from MTA)

Deep seismic studies

In Soros Gulf, Turkey Petroleum Corporation (TPAO) are made by deep seismic survey north to south SRZ-5 SRZ-7 is called SRZ-8 (Figure 6A). When the seismic sections are examined, it is understood that the slope of the Ganos Fault, which forms the western end of the Saros Graben, is steeper than the faults at the northern end. Shallow seismic data in the region also proves this phenomenon. When examining Figure 6A, it is possible to examine the deep seismic sections by dividing them into 3 units. Unit 2 in the basin of the Saros Gulf basin, which has a sigmoidal-oblique reflection of a delta sediment in the seismic sections on the shelf, may be the equivalent of Unit 1 in this project on the southern shelf of the Gulf. It is not possible to have a counterpart at the base, which may point to an environment of the same kind, even at low sea level during glacial periods, as the bottom of the bay will be covered with water (18). There is a possibility that Unit 2 on Unit 2 shelf at the base of the bay may be a possible correlating reservoir (18). Unit 3 on the shelf is considered the equivalent of Unit 3 and older sediments observed at the bottom of the basin (18). High resolution shallow seismic study is given in Figure 6B. Again, in this section, the boundaries of the two units are clearly seen.

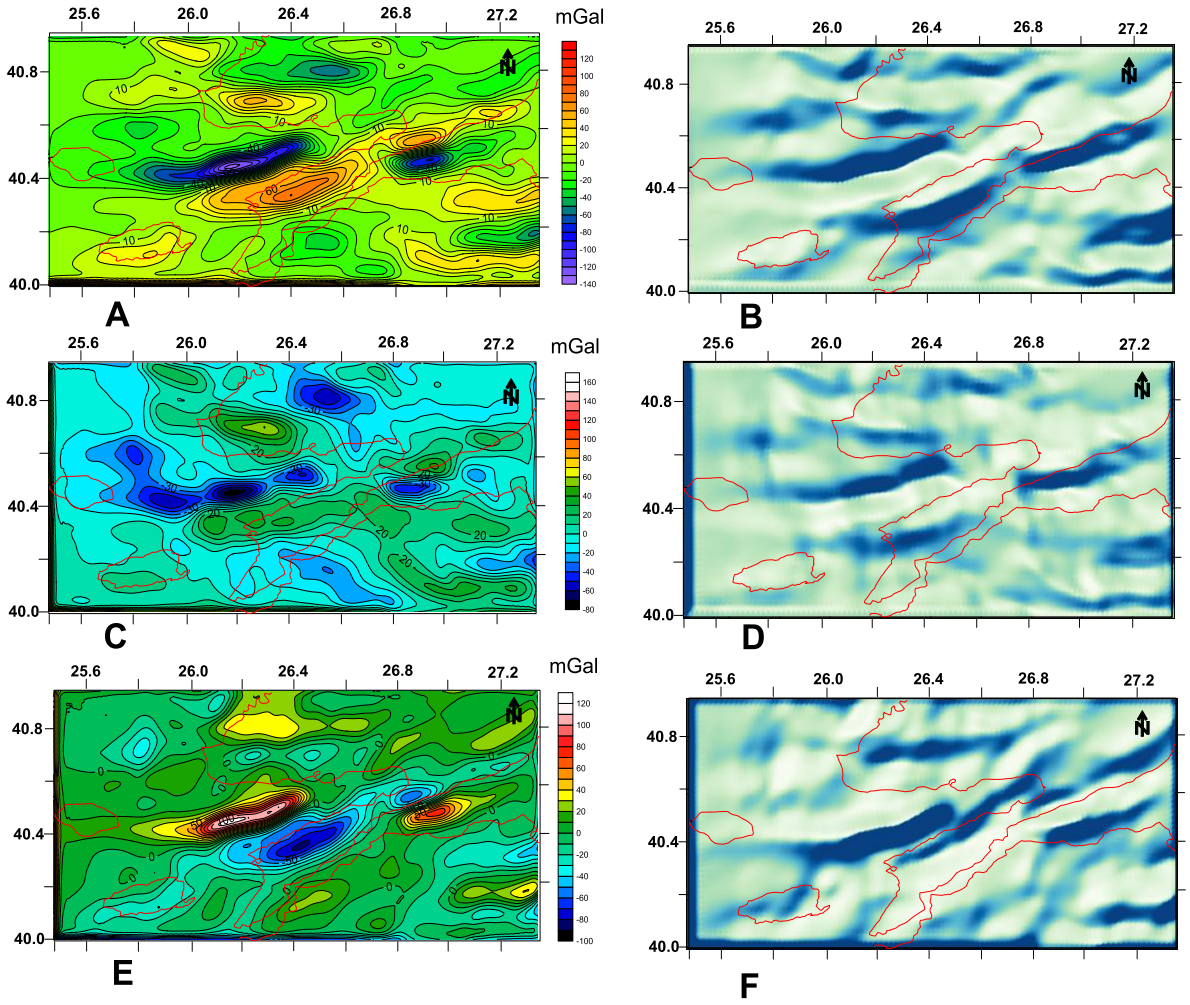

Figure 5: The output of residual anomaly map obtained after applying the guided filter method of Bouguer anomaly map of Saros Gulf. C) anomaly map in 45^0 D) Shaded Relief image of anomaly map in 45^0. E) 135^0 anomaly map F) Shaded Relief image of 135^0 anomaly map

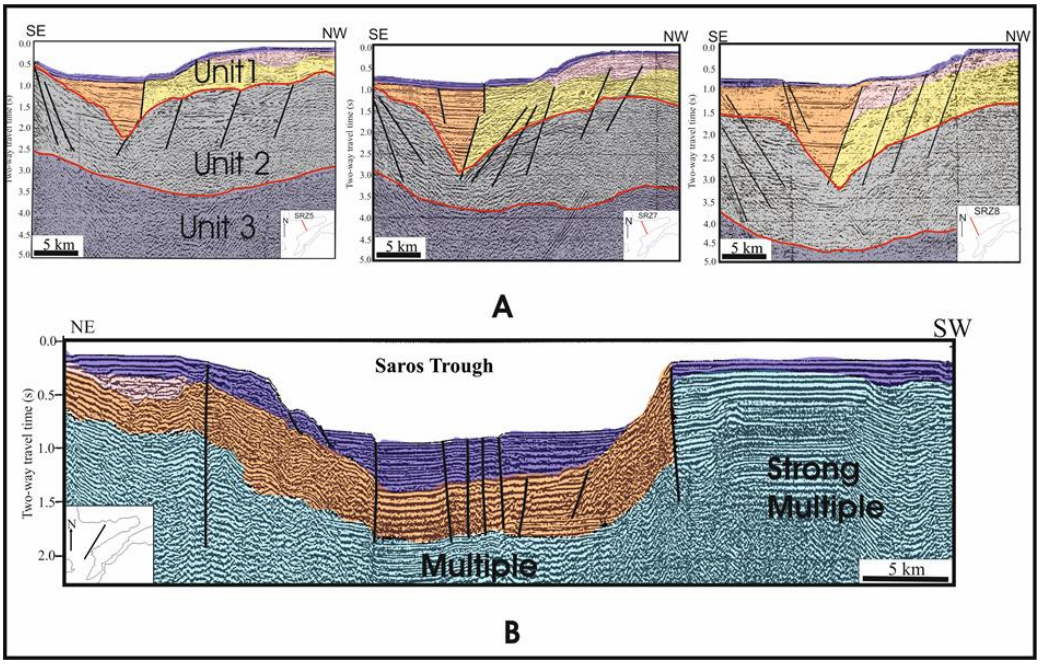

Figure 6: Seismic sections in Gulf of Saros show two difference depth information in seconds. A) Depth seismic sections (modified from TPAO). B) High resolution seismic section of shallow part of the region (modified from [18]).

From the seismic sections, the Upper Miocene unit at the bottom of the sequence and Units 1, 2, and 3, which are located on the basement, are marine sediments deposited between 13 thousand years and today, and interglacial marine intercalations between delta and Riss-Würm deposited 25-13 thousand years ago. They have shown that the provision. This stratigraphic sequence suggests that it continues at the southern shelf of the gulf and at the base of the Saros basin [15]. Although it is stated that the seismic stratigraphic sequence in the northern shelf of the gulf continues in the southern shelf of the Dardanelles at the Aegean Sea, it is suggested by several authors that delta sediments (Unit 2) can be represented temporally by the correlated marine sediments [15].

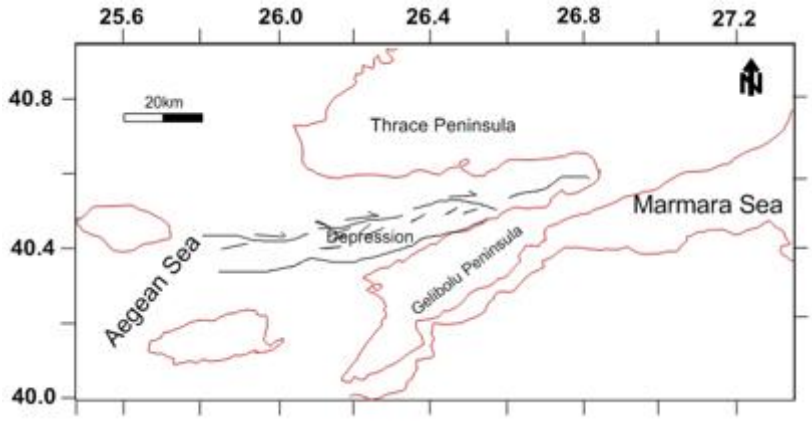

Figure 7: Proposed active fault map of the study area.

Results and Discussion

The aim of this study is to determine the structural boundaries of the potential field data and to make the regional-residual distinction of the potential field data. For this purpose, it is aimed to illuminate the complex tectonics of Saros Gulf by using a Steerable filter method. Gravity anomaly maps in the region (Figure 4) were interpreted separately by applying Steerable Filter method (Figure 5). When Bouguer anomaly is examined, there is a strong effect in Saros Gulf. Bouguer anomaly maps can Steerable Filter method to map obtained after

applying anomalies Turkey Petroleum Corporation (TPAO) received by comparison with the deep and shallow seismic data were made. When the seismic activity of the region (Figure 3) and the deep and shallow seismic sections obtained by TPAO (Figure 6) are examined, it can be said that the region consists of many active faults. They also identified 69 genera of folaminifera in the current Benthic and Planktic Foraminifera [7, 22]. These folaminifers were able to survive with the effects of hot water from the faults and were concentrated in places where these faults exist [7]. When all these data are evaluated, it is seen that the fault lines in the bay provide a very consistent overlap with the map obtained after the application of the Steerable Filter method to the gravity anomaly maps. All these data were examined and interpreted to obtain a map of the tectonic structure and fault lines of the Saros Gulf (Figure 7).

Acknowledgments

İn this study, we lent their support from the Mineral Research and Exploration İnstitute (MTA) and Turkey Petroleum Corporation (TPAO), thank you to their employees.

References

[1]. Elmas, A., & Meriç, E (1998). The Seaway Connection between the Sea of Marmara and the Mediterranean: Tectonic Development of the Dardanelles, *International Geology Review*, (40): 144-162.

[2]. Girgin, A (2010). İnvestigation of Saros Gulf by Geophysical Methods. İstanbul University, İnstitute of Science and Technology. *Master Thesis*. İstanbul.

[3]. Freeman, WT., & Adelson, EH (1991). The Design and Use of Steerable Filters, *İEEE Trans. On Patt. Anl. and Machine İntell*, (13): 891-906.

[4]. Laine, AF., & Chang, CM (1995). De-Noising Via Wavelet Transforms Using Steerable Filters, *Proc. İeee İnt. Sym. On Circuits and Systems*, (3): 1956-1959.

[5]. Özmen, A (2001). Cellular Artificial Neural Networks and İmage Processing Applications, İstanbul University, İnstitute of Science, *PhD Thesis*, İstanbul.

[6]. Ucan, ON., Albora, AM., & Ozmen, A (2003). Evaluation of Tectonic Structure of Gelibolu (Turkey) Using Steerable Filters. *Journal of the Balkan Geophysical Society*, (6): 221–234.

[7]. Albora, AM., Meriç, E., Avşar, N., & Uçan, ON (2005). Evaluation of Seismic, Gravity and Magnetic Data of Gulf of Saros and their Correlation with Bentick Foraminifers. *Applied Geosciences-Kocaeli University*, (5): 1-15.

[8]. Sari, C., Özel, E., & Ergun, M (1995). Tectonics and Structure of the Saros Bay Area, *Nezihi Canitez Symposium, Journal of Geophysics*, (9): 89-96.

[9]. Cramplin, S., & Evans, R (1986). Neotectonic of the Marmara Sea Region in Turkey, *Jour. Geol. Soc. Lond.*, (143): 343-348.

[10]. Barka, AA., & Kadinsky-Cade, K (1988). Strike-Slip Fault Geometry İn Turkey and İts İnfluence on Earthquake Activity, *Tectonics*, (7): 663-684.

[11]. Saner, S (1985). Therefore the Gulf of Saros precipitation truck and Tectonic placement, Northeastern Aegean Sea, *Turkey Geological Society Bulletin*, (28): 1-10.

[12]. Mckenzie, DP (1978). Active Tectonics of the Alpine-Himalayan Belt: The Aegean Sea and Surrounding Regions, *Geophys. Jour. Royar Astron. Soc*., (55): 217-254.

[13]. Albora, AM., Uçan, ON., & Hisarli, ZM (2001). Interpretation of Gravity and Magnetic Anomaly Maps of Saros Gulf and Gökçeada Region by Wavelet Approach, Turkish Marine Research Foundation, *Tudav-Gökçeada*, 23-36.

[14]. Uçan, ON., Albora, AM., & Özmen, A (2003). Application of Cellular Artificial Neural Networks Approach to Saros Bay Gravity Anomaly Map, *Journal of Applied Geosciences (Turkey)*, (3): 91-99.

[15]. Çağatay, MN., Görür, N., Alpar, B., Saatçilar, R., Akkök, R., Sakınç, M., Yüce, H., Yaltırak, C., & Kuşcu, I (1998). Geological evolution of the Gulf of Saros, NE Aegean Sea. *Geo Mar Lett*, (18): 1–9.

[16]. Taymaz, T., Jackson, J., & Mckenzie, D (1991). Active tectonics of the North and central Aegean Sea, *Geophy. Jour. İnt.,* (106): 443-490.

[17]. Karabulut, H., Roumelioti, Z., Benetatos, C., Mutlu, A.K., Özalaybey, S., Aktar, M., & Kiratzi, A (2006). A source study of the 6 July 2003 (Mw 5.7) earthquake sequence in the Gulf of Saros (Northern Aegean Sea): Seismological evidence for the western continuation of the Ganos fault. *Tectonophysics*, (412): 195-216.

[18]. Ustaömer, T., Gökaşan, E., Tur, H., Görüm, T., Batuk, GF., Kalafat, D., Alp, A., Ecevitoğlu, B., & Birkan, H (2008). Faulting, mass-wasting and deposition in an active dextral shear zone, the Gulf of Saros and the NE Aegean Sea, NW Turkey, *Geo-Marine Letters*, (28): 171-193.

[19]. Tüysüz, O., Barka, A., & Yiğitbaş, E (1998). Geology of the Saros Graben and İts İmplications for the Evolution of the North Anatolian Foult in the Ganos-Saros Region, Nortwestern Turkey, *Tectonophysics*, (293): 105-126.

[20]. Makris, J (1977). Geophysical İnvestigations of the Helle-Nides, *Hamb. Geophys. Einzelschriften*, (34): 1– 124.

[21]. Brooks, M., & Kiriakidis, L (1986). Subsidence of the North Aegean Trough, An Alternative View, *J. Geol. Soc. Lond.*, (143): 23–27.

[22]. Meriç, E., Avşar, N. & Bergin, F (2004). Benthic foraminifera of Eastern Aegean Sea (Turkey) systematics and autoecology. *Turkish Marine Research Foundation and Chamber of Geological Engineers of Turkey*, (18): 306 p.